ACS APPLIED ELECTRONIC MATERIALS

pubs.acs.org/acsaelm

Forum Article

Screening and Design of Bipolar Magnetic-Semiconducting Monolayers and Heterostructures

Jun Deng, Jinbo Pan, Yanfang Zhang, Yuhui Li, Wenhan Dong, Jiatao Sun, and Shixuan Du*

Cite This: ACS Appl. Electron. Mater. 2022, 4, 3232−3239

Read Online

ACCESS | Metrics & More | Article Recommendations | Supporting Information

ABSTRACT: Bipolar magnetic semiconductors (BMSs) show great promise in spintronic devices because of their spin-dependent transport properties. Two-dimensional (2D) BMSs with electrically controllable spin polarization are ideal materials for bipolar manipulating the spin orientations at the nanoscale. Here, we systematically screened 2D BMSs from the 2DMatPedia database and found 11 promising candidates from 6531 structures. We attribute the formation of BMS electronic structure to the strong crystal field effect and low spin-exchange splitting in these structures. Moreover, we proposed an alternative way to construct BMS via engineering of heterostructures. The unique electronic structures of BMS can be achieved by stacking two half semiconductors with interlayer antiferromagnetic coupling and type-II band alignment. This approach was verified in CrI_3/VI_3 and CrSCl/CrSBr bilayer systems. Our work not only provides potential candidates of BMSs but also gives insight into the formation mechanism of BMSs, which will stimulate the experimental synthesis and application of BMSs.

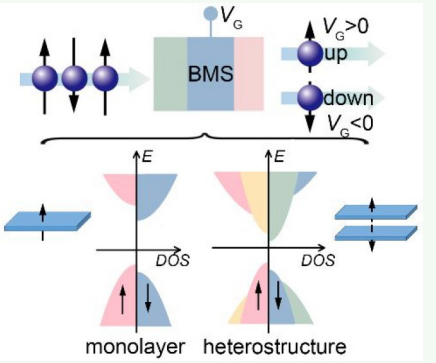

KEYWORDS: *2D bipolar magnetic semiconductors, high-throughput calculations, heterostructures, crystal field effect, spin-exchange interaction*

INTRODUCTION

Spintronics, utilizing the spin degree of electrons, has attracted researchers' interest for its applications in information storage, logic devices, and tunnel transistors. The fabrication of two-dimensional (2D) magnetic materials opens the doors for spintronic devices at the nanoscale. However, generation of polarized spin current and spin manipulation/detection are still challenges in this field.[1] The concept of half metal was proposed hereafter, in which one of the spin channels is metallic and the other is insulating.[2] Thus, it can provide 100% spin-polarized current. In recent years, a more ideal material, bipolar magnetic semiconductor (BMS), was put forward to meet the requirement of spin manipulation.[3,4] In contrast to fixed spin-polarization in half metals, the spin orientations of BMS can be reversibly tuned by an electric-field. This is due to the unique band structure of BMS, in which the band structure splits into two sub-bands with opposite spin directions for VBM and CBM. Thus, by electron/hole doping, it will become a half-metal with spin-up/spin-down carriers at the Fermi level. They have potential applications in spin filter, spin valve, or spin separators.[3,4] In the past few years, several 2D BMSs were theoretically predicted, including $MnPSe_3$ nanosheet,[5] Janus MXene,[6] monolayer NbS_2,[7] MoI_3,[8] and a DPP-based metal−organic framework.[9] While, the experimentally synthesized 2D magnetic semiconductors CrI_3[10] and $CrGeTe_3$[11] are half semiconductors (HSCs) whose VBM and CBM belong to the same spin channel.[12] Until now, the experimental realization of BMS is still lacking, which hinders its application in spintronics. Thus, it is emergent to search and design experimentally reachable 2D BMSs.

With the development of material science, several 2D materials databases are constructed through high-throughput calculations, e.g., C2DB,[13] 2DMatPedia.[14] Abundant materials with desired chemical and physical properties were screened out by utilizing these databases. For example, Liu et al. discovered several 2D materials with topological flat bands in the 2DMatPedia database;[15] Yang et al. identified 9 potential 2D catalysts for the hydrogen evolution reaction.[16] It should be mentioned that in a recent work, Wang and co-workers screened out 11 BMSs from the Materials Project database,[17] but in a three-dimensional form. Therefore, searching from the 2D materials databases is an effective way to discover 2D BMSs. Another way is to create BMS by stacking the experimentally realized 2D magnetic semiconductors. This idea is stimulated by a recent report, in which a magnetic semiconductor with a topologically nontrivial band structure

Special Issue: 2D Magnetism - Materials, Devices, and Applications

Received: April 11, 2022
Accepted: June 1, 2022
Published: June 16, 2022

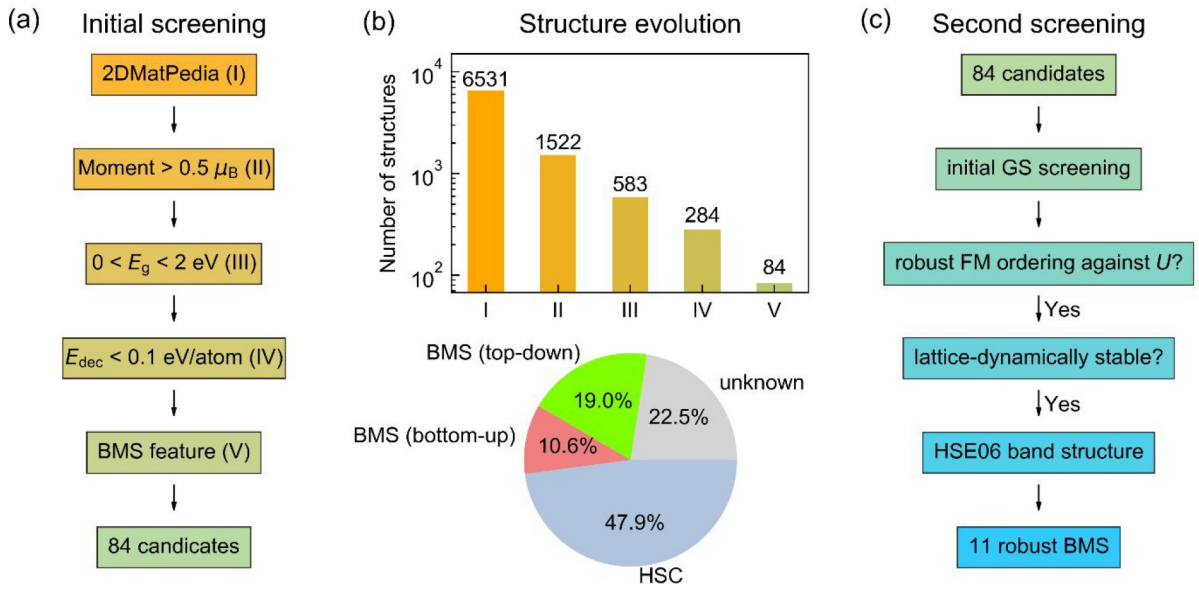

Figure 1. High-throughput screening flow of BMSs. (a) Initial screening flow from the 2DMatPedia database. (b) The upper panel shows the structural evolution in the corresponding step in part a. The lower panel shows the structural distribution of the 284 energy favorable structures. (c) Second screening flow for the 84 candidates in the initial screening.

could be produced by stacking two topologically trivial ferromagnetic semiconductors.[18]

In this Forum Article, we screened out BMSs from the 2DMatPedia database and proposed a design principle for BMSs. By searching from the 2DMatPedia database and high-throughput calculations, we screened out 11 BMSs with robust ferromagnetism and high stability. Three of them are experimentally synthesized, and two of them are suitable for bipolar doping. By analyzing their electronic structures, we conclude that the strong crystal field effect and low spin-exchange splitting are responsible for the observed BMS property for them. Moreover, we proposed that BMS can be obtained by stacking two HSCs with interlayer antiferromagnetic coupling and type-II band alignment, which was verified in CrI_3/VI_3 and CrSCl/CrSBr bilayer systems. Our work will stimulate the experimental realization and application of BMS in spintronics.

COMPUTATIONAL METHODS

The first-principles calculations were carried out with the density functional theory (DFT) implemented in the Vienna *ab initio* simulation package (VASP).[19] For high-throughput screening BMSs from the 2DMatPedia database,[14] we adopted the generalized gradient approximation (GGA) in the form of the Perdew–Burke–Ernzerhof (PBE)[20] for the exchange-correlation potentials. The projector-augmented-wave (PAW)[21] pseudopotentials were used with a plane wave energy of 520 eV. The GGA+U method with Dudarev's approach[22] was applied for transition metal oxides and fluorides for the initial ground state identification, where the effective U parameter $U_{eff} = U - J$ values were chosen as default values in the pymatgen package.[23] A Monkhorst–Pack[24] Brillouin zone sampling grid with a resolution of $0.02 \times 2\pi$ Å^{-1} was applied. A 20 Å vacuum layer was used to avoid the interlayer interactions along the c direction. For each magnetic structure, atomic positions and lattice parameters were relaxed until all the forces on the ions were less than 10^{-2} eV/Å. The electronic structures were calculated with a hybrid functional HSE06,[25] where a mixing parameter of 25% was adopted for the exact-exchange term. Phonon spectra were calculated using the finite displacement method implemented in the PHONOPY code[26] to determine the lattice-dynamical stability of the structures. For heterostructures, optB86b functional[27,28] was used to consider the van der Waals interlayer interaction. A cutoff energy of 700 eV was adopted. The on-site Coulomb interaction U_{eff} of the d orbital of Cr and V are chosen as 2.8 eV (U = 3.9 eV, J = 1.1 eV) and 3.68 eV (U = 3.68 eV, J = 0 eV) for CrI_3/VI_3 heterostructure, respectively. These U values were determined with a linear response method.[29−31] For the CrSCl/CrSBr bilayer system, the Hubbard U term was switched off, for it can better describe the interlayer coupling for bulk CrSBr, which is discussed in Note 1 in the Supporting Information.

RESULTS AND DISCUSSION

We started from the 2DMatPedia database,[14] which contains 6531 entries and 5279 electronic structures. Figure 1 shows our workflow for searching potential BMSs. To screen out BMSs, only ferromagnetic (FM) semiconductors with magnetic moments larger than 0.5 μ_B, bandgap E_g between 0 and 2 eV (0 eV < E_g < 2 eV), and decomposition energy E_{dec} less than 0.1 eV/atom were considered as potential candidates. Here, the decomposition energy E_{dec} is defined as the energy required to decompose the compound to its most stable materials.[14] There are 284 materials satisfying the criteria. Further screening the materials with the BMS property results in 84 candidates. The number of structures in each screening condition is shown in the upper panel of Figure 1b. The bottom panel in Figure 1b shows the structural distribution of the 284 semiconductors. Nearly half of the energetically favorable structures are HSCs and 29.6% of them are BMSs, where 10.6% are BMSs from the top-down approach and 19% are BMSs from the bottom-up approach. Here, the structures from the top-down approach are exfoliated from existing layered materials, while those from the bottom-up approach are obtained by chemical substitution of those from the top-down approach. The electronic structures of the 22.5% structures have not been calculated in the database. Therefore, we do not take them into consideration.

Then, a second screening was adopted to confirm the BMS character of the 84 candidates. As only FM configuration was considered for magnetic materials in the 2DMatPedia database, the ground states (GS) of them need to be further investigated.

https://doi.org/10.1021/acsaelm.2c00464
ACS Appl. Electron. Mater. 2022, 4, 3232−3239

Table 1. Four Prototypes of the Screened 11 BMSs

Prototype	CuF_2	TaS_2	Nb_3Br_8	$CdCl_2$
Top view	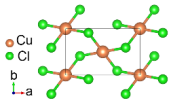	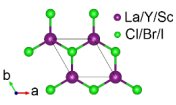	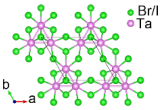	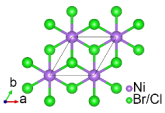
Side view	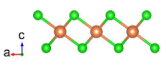		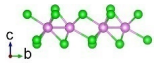	
Chemical Formula	$CuCl_2$	$YBr_2/YCl_2/LaBr_2$ $ScCl_2/ScBr_2/ScI_2$	Ta_3Br_8/Ta_3I_8	$NiCl_2/NiBr_2$
Space group	$P2_1/c$	$P\bar{6}m2$	$P3m1$	$P\bar{3}m1$

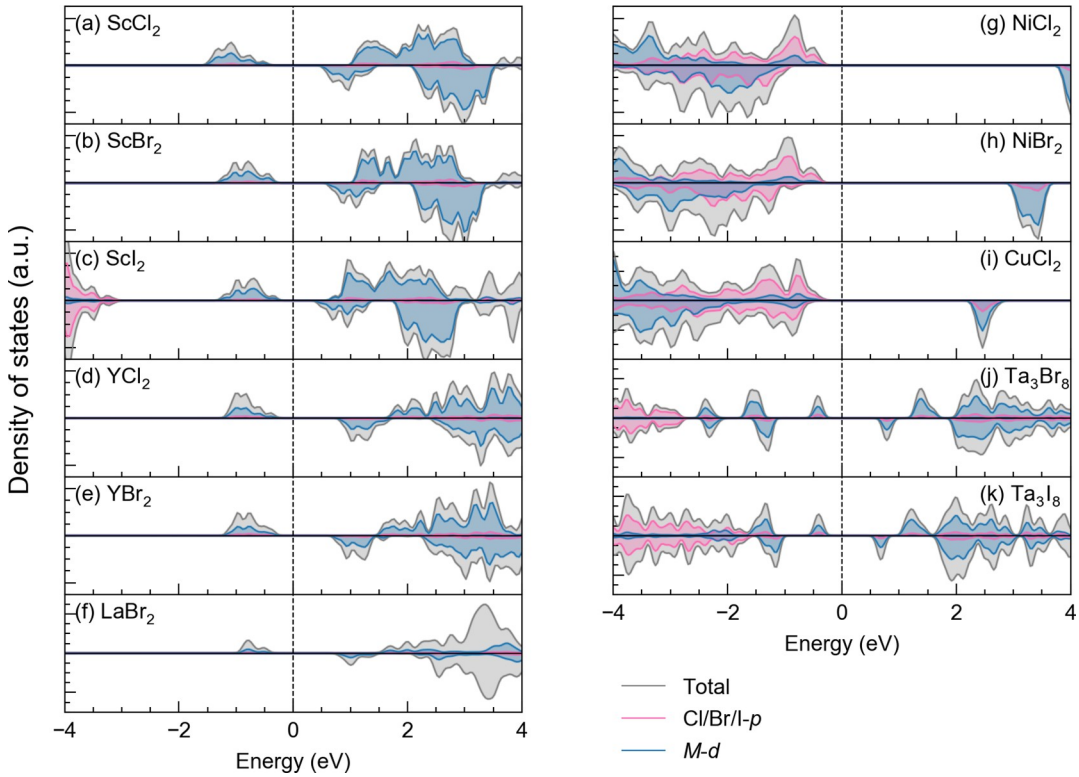

Figure 2. Density of states for the 11 BMS candidates: (a) $ScCl_2$, (b) $ScBr_2$, (c) ScI_2, (d) YCl_2, (e) YBr_2, (f) $LaBr_2$, (g) $NiCl_2$, (h) $NiBr_2$, (i) $CuCl_2$, (j) Ta_3Br_8, and (k) Ta_3I_8, where the Fermi level was set to zero. The *M* in the legend represents magnetic elements in the compounds, where *M* = Sc/Y/La/Ni/Cu/Ta. The HSE06 functional was adopted here.

We first generated different magnetic configurations for them as described in Note 2 in the Supporting Information and compared the total energies to identify the ground state. Only ferromagnetic semiconductors were left. Then we checked the robustness of the FM ordering of them against a serial of Hubbard U_{eff}, which accounts for the strong correlation of d/f electrons, and the results are demonstrated in Figures S1 and S2. Next, phonon dispersions were calculated for the remaining ones to confirm their lattice-dynamical stabilities (see Figure S3). Finally, HSE06 functional was adopted to calculate their electronic structures. After these procedures, the 11 most promising BMSs were screened out.

Table 1 shows the crystal structures of the screened 11 BMSs. These materials can be further categorized into four structural types: CuF_2 type, H-TaS_2 type, Nb_3Br_8 type, and $CdCl_2$ type. In these materials, monolayer $NiCl_2$ and $LaBr_2$ are predicted to be easily exfoliated from their layered bulk form,[32,33] and monolayer $NiBr_2$ has been experimentally achieved.[34] The others are theoretical predictions. Their lattice parameters are summarized in Table S1. We noticed that some of them have been predicted elsewhere with high Curie temperatures.[35] Then, the electronic structures are investigated with an HSE06 functional. The density of states of them are displayed in Figure 2, and the corresponding electronic structures are summarized in Figure S4. It is obvious that all of them are spin-polarized and have opposite spin directions for CBM and VBM, which is the main characteristic of BMS. We note that monolayer $NiBr_2$ has a helimagnetic order below 27 K in experiment,[34] indicating that $NiBr_2$ is not a good candidate for BMS.

Now, we try to get insight into the formation mechanism of BMS for these candidates. The BMS feature of them can be

https://doi.org/10.1021/acsaelm.2c00464
ACS Appl. Electron. Mater. 2022, 4, 3232−3239

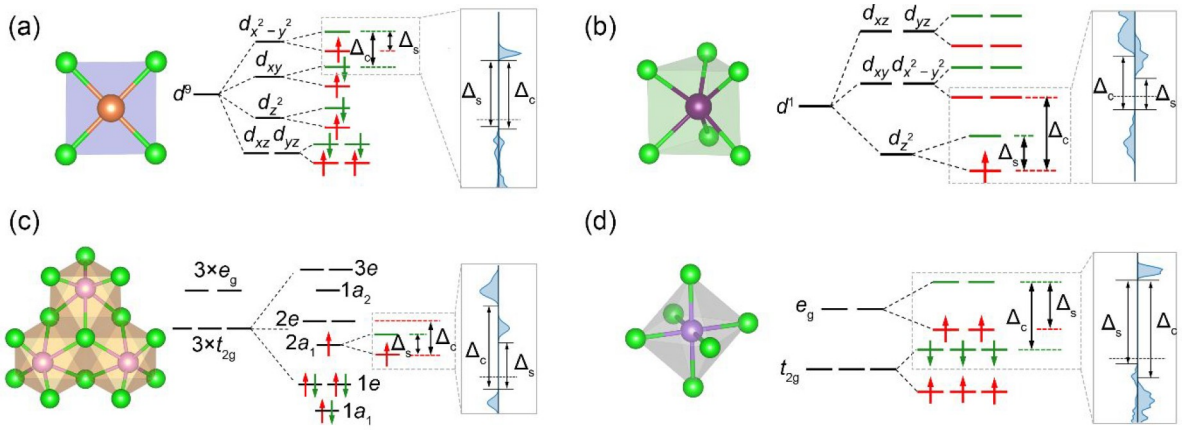

Figure 3. Schematic diagram of atomic coordination (left), energy levels and electron occupation of d orbitals (middle), and density of states (right) for (a) $CuCl_2$, (b) $YBr_2/YCl_2/LaBr_2/ScCl_2/ScBr_2/ScI_2$, (c) Ta_3Br_8/Ta_3I_8, and (d) $NiCl_2/NiBr_2$. Here, Δ_c is the gap induced by crystal field splitting and Δ_s is the spin gap caused by spin-exchange interaction. The right panel of each subgraph shows the projected density of states of d orbitals for $CuCl_2$, $ScCl_2$, Ta_3Br_8, and $NiCl_2$ for a direct comparison with the middle schematic diagram.

understood from the crystal field theory point of view. Here, we take $CuCl_2$ as an example. Figure 3a shows the atomic coordination of Cu in $CuCl_2$. Under the square planar crystal field, the d orbitals of Cu split into four groups: d_{xz}/d_{yz}, d_{z^2}, d_{xy}, and $d_{x^2-y^2}$ with splitting energy Δ_c. Due to the spin-exchange interactions, these energy levels further split into spin-up and spin-down subgroups with a spin-exchange splitting Δ_s. Thus, under the electron configuration of Cu-$3d^9$, one unpaired electron occupies the spin-up channel of the $d_{x^2-y^2}$, leading to a magnetic moment of 1.0 μ_B/formula. The BMS band structure forms as the crystal field splitting Δ_c is larger than the spin-exchange splitting Δ_s. Here, Δ_c is the gap between the d_{xy} and the $d_{x^2-y^2}$ of the spin-down channel, and Δ_s is the gap between spin-up and spin-down channel of the $d_{x^2-y^2}$ orbital. The other compounds can be explained in a similar way. In the H-TaS_2 structural type, the d orbitals of Sc/Y/La in $ScCl_2/ScBr_2/ScI_2/YCl_2/YBr_2/LaBr_2$ split into d_{z^2}, $d_{xy}/d_{x^2-y^2}$, d_{xz}/d_{yz} under a triangular prism crystal field with one electron occupying the lowest d_{z^2} of the spin-up channel. In the Nb_3Br_8 structural type, the d orbitals of Ta in Ta_3Br_8/Ta_3I_8 split into t_{2g} ($d_{xy}/d_{xz}/d_{yz}$), and e_g ($d_{x^2-y^2}/d_{z^2}$) under the octahedral crystal field. These orbitals further split into 1e, 1a_1, 2e, 2a_1, 3e, 1a_1 energy levels due to the formation of the Ta_3Br_{13}/Ta_3I_{13} cluster with one electron occupying the spin-up channel and an unoccupied 2a_1 orbital in the spin-down channel.[36] In $CdCl_2$ structural type, the d orbitals of Ni in NiX_2 (X = Cl, Br) split into t_{2g} ($d_{xy}/d_{xz}/d_{yz}$), and e_g ($d_{x^2-y^2}/d_{z^2}$) under the octahedral crystal field. The t_{2g} orbitals are fully occupied and two electrons occupy e_g orbitals of the spin-up channel. The common feature of them is that the electronic states of the magnetic atoms in VBMs and CBMs come from the same orbital but belong to different spin channels caused by spin splitting exchange interaction. This is confirmed by the electron density of their valence band and conduction band (Figure S5), which show the corresponding orbital characters (e.g., $d_{x^2-y^2}$ orbital shape for Cu in $CuCl_2$, d_{z^2} orbital shape for La in $LaBr_2$). The bandgaps of them are mainly determined by the spin-exchange splitting Δ_s rather than crystal-field-induced gap Δ_c, because Δ_s is always smaller than Δ_c for the 11 BMS candidates. This is coincident with a previous report that the strength of on-site Coulomb repulsion and the crystal field effect plays an important role in the formation of BMSs.[37] Here, we summarize that choosing 4d/5d transition metals and ligands with large electronegativity can effectively reduce spin-exchange splitting, enhance crystal field splitting, and consequently lead to the formation of BMS.

For practical applications, the key to realizing bipolar manipulation in experiments, i.e., both electron and hole doping, is determined by electron affinity (EA, $E_{CBM} - E_{vac}$) and ionization potential (IP, $E_{VBM} - E_{vac}$), where E_{vac} is the vacuum energy. The deeper the IP is, the harder the electron can escape from the material; the shallower the EA is, the more difficult the electron can dope into the material. Hosono et al. summarized that electron doping can be achieved when EA is lower than −3.8 eV and hole doping is easy when IP is higher than −6 eV.[38] The calculated EAs and IPs for the BMS candidates are summarized in Figure S6. Ta_3Br_8/Ta_3I_8 have proper EA and IP that is appropriate for bipolar doping, where the CBM and VBM are located at −3.68 eV/−3.65 eV and −4.74 eV/−4.58 eV, respectively.

Despite our endeavor to search 2D BMSs in the database, this kind of materials are still rare in the monolayer form, especially with high tunability and suitable band edges. Figuring out a design principle for BMS is highly important. It should be noted that the most screened out 2D magnetic semiconductors are HSCs. It is desirable to create BMSs from these HSCs. Inspired by a recent report about construction of topologically nontrivial magnetic semiconductor by stacking two topologically trivial FM semiconductors,[18] we stack two HSCs with intralayer FM ordering to form a heterostructure with type-II band alignment. In this heterostructure, the CBM is from one layer while the VBM is from the other layer. Usually, the interlayer coupling is weak and does not influence the intralayer coupling. Two cases may occur according to the interlayer coupling. The first one is that the interlayer coupling is antiferromagnetic (AFM). In this case, the CBM and VBM of the heterojunction belong to two opposite spin channels, which is the desired BMS shown in Figure 4a. The second case is that the interlayer coupling is FM. In this case, the heterojunction is still an HSC, in which the VBM and CBM are from the same spin channel (Figure 4b).

To verify our hypothesis, we choose the van der Waals FM semiconductors CrI_3 and VI_3 as an example, which were experimentally synthesized.[39−41] The bulk phase of VI_3 and CrI_3 are layered materials with similar structures: at high temperature (HT), they adopted the $C2/m$ space group, and at low temperature (LT), they crystallize with the $R\bar{3}$

https://doi.org/10.1021/acsaelm.2c00464
ACS Appl. Electron. Mater. 2022, 4, 3232−3239

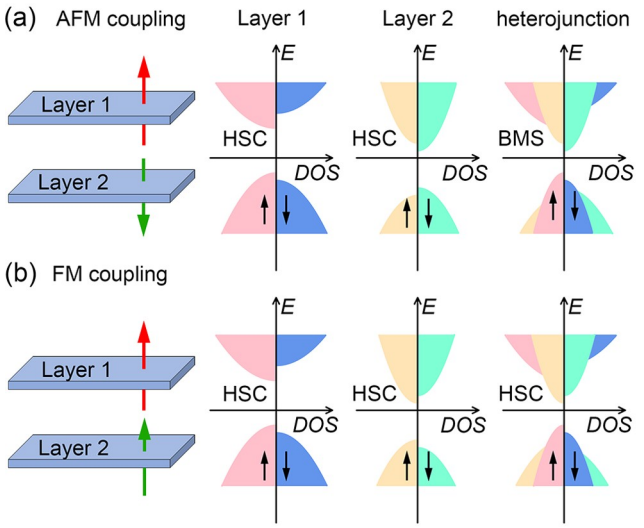

Figure 4. Schematic diagram for designing BMS by layer stacking. Here, we consider two half-magnetic semiconductors (HSCs) with type-II band alignment, namely, the CBM and VBM come from different layers. (a) When interlayer coupling is AFM, the heterojunction is a BMS, where CBM and VBM have opposite spin directions. (b) When the interlayer coupling is FM, the heterojunction is still an HSC.

structure.[39−41] The difference between the HT and LT structures lies in the stacking ordering, and the intralayer structure is nearly intact. Moreover, at LT, both of them are ferromagnets, which are considered as Ising magnets.[39,41,42] The monolayer form of them is predicted to be FM semiconductors with HSC band structures,[12,41,43−45] though monolayer VI_3 has not been obtained yet to the best of our knowledge. We also reproduced the insulating state for monolayer VI_3 to ensure the validation of our simulations (see Note 3 in the Supporting Information).

We constructed CrI_3/VI_3 heterostructures with the low-temperature AB and high-temperature AC_1 stacking modes shown in Figure 5a,b, where the mismatches are less than 0.6%. The AC_1 stacking mode can be obtained by shifting the upper layer of the AB stacking structure with a vector of $1/3\ \vec{b}$. By comparing the total energies of interlayer-FM and interlayer-AFM coupling for these two stacking modes, we found that the ground state of AB stacking is FM, while that of AC_1 stacking ordering is AFM. The electronic structures of them are shown in Figure 5c,d, respectively. It proves our assumption that FM stacking of HSCs leads to HSC, while AFM stacking of HSCs produces a BMS. Besides, the projected band structure (Figure S7) shows that the CBM is mainly contributed by VI_3, and VBM contributed by CrI_3, which is indeed a type-II heterojunction. We further examined the influence of spin−orbit coupling (SOC) on the band structure for AC_1 stacking structure. As shown in Figure S8, though the band degeneracies at some K points are broken, the spin states of the CBM and VBM do not change. Besides, we found that the interlayer coupling of AC_1 stacking mode is sensitive to Hubbard U values (Figure S9), which is also found in bilayer VI_3.[44] We notice that the AFM ground state can be obtained by using the U values adopted in Materials Project[46] and those from linear response method.[29,30] Here, the U values we used were calculated by the linear response method.

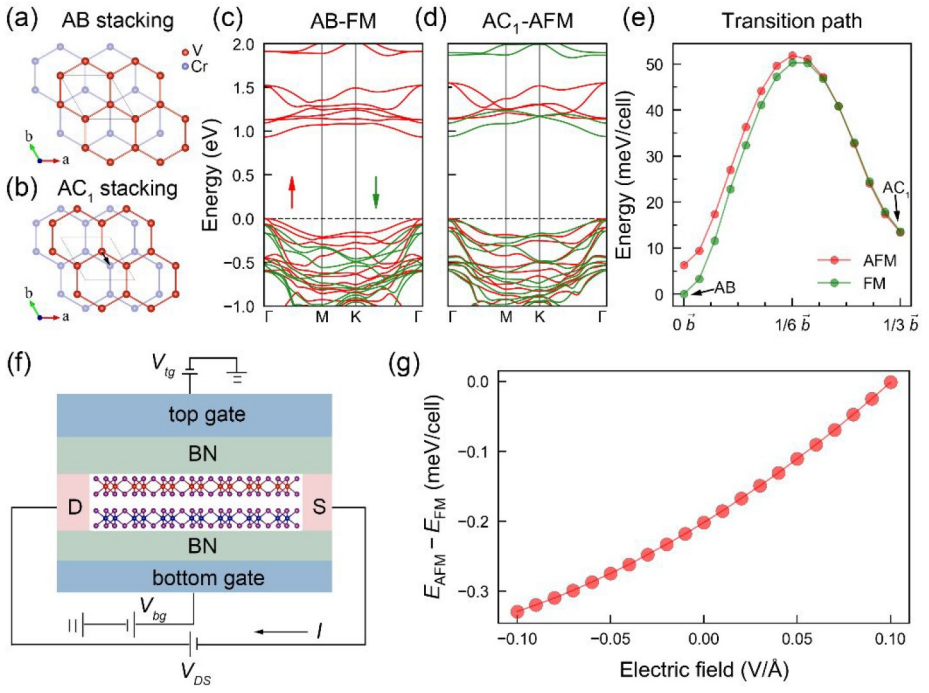

Figure 5. (a) AB stacking and (b) AC_1 stacking of the CrI_3/VI_3 heterojunction. Here, I atoms are omitted for clarity. AB stacking ordering can be obtained by shifting the upper layer of AC_1 stacking structure with a $-1/3\ \vec{b}$ vector indicated in part b. (c,d) Spin resolved band structures for AB and AC_1 stacking ordering, respectively. The ground state FM coupling for AB and AFM coupling for AC_1 stacking was adopted. (e) Transition path from AB to AC_1 stacking. The z-axis of every atom was relaxed and the others are fixed. The spin−orbit coupling was ignored here. (f) Supposed electric field transistor with top and bottom gates. (g) The energy difference between interlayer the FM and AFM configuration under an electric field.

https://doi.org/10.1021/acsaelm.2c00464
ACS Appl. Electron. Mater. 2022, 4, 3232−3239

By comparing the total energies of the AB and AC_1 stacking structures, we found that AB stacking ordering is more stable than that of AC_1 stacking, indicating that AC_1 is a metastable stacking ordering, consistent with the reference.[47] We further calculated the transition path from AB to AC_1. The result is shown in Figure 5e. Similar to the result of bilayer CrI_3,[29] there is a barrier around 38 meV/cell in the transition path, which may hinder the sliding from AC_1 to AB stacking. Thus, we believe that AC_1 stacking can be achieved in the experiment.

In manipulating the spin direction of BMSs, applying a gate voltage is a direct way to tune the Fermi level and change the doping type. For heterostructures, i.e., the CrI_3/VI_3 bilayer here, it is crucial to control the doping type separately for each layer, because the VBM and CBM come from different layers. Here, we propose to use a field effect transistor with both the top gate and bottom gate to separately dope different carriers into each layer by the electric field (see Figure 5f). It is supposed that the system is electron-doped for the top layer when $V_{tg} > V_{bg}$, while it is hole-doped for the bottom layer when $V_{tg} < V_{bg}$. We then calculated the ground state of CrI_3/VI_3 bilayer under a finite electric field. By applying a forward and backward electric field, the system keeps the interlayer AFM state as shown in Figure 5g. Thus, the AFM state is robust against the electric field (within ±0.1 eV/Å). Also, the spin direction of the CrI_3/VI_3 bilayer can be tuned under the field effect transistor.

Another example is the CrSCl/CrSBr bilayer system. Both CrSCl and CrSBr are HSCs with intralayer FM coupling (see Note 4 in the Supporting Information), in good agreement with previous reports.[35,48,49] The lattice mismatch of the CrSCl/CrSBr bilayer we constructed is less than 3%. Under interlayer FM coupling, the bilayer system is still an HSC. Also, it becomes a BMS with interlayer AFM coupling. The electronic structures of them are shown in Figure S10. This again verifies our proposed design method of BMS. However, the energy difference between FM and AFM interlayer coupling is tiny and is sensitive to strains (see Note 4 in the Supporting Information), suggesting that it is not a robust BMS. However, it indicates that we can tune the interlayer coupling by introducing strain. Moreover, this tunable band alignment induced by switchable interlayer magnetism makes it a promising material for spin-constrained optoelectronic application and photoexcitation induced spin carrier injection.[50,51]

CONCLUSIONS

In summary, by high-throughput calculation, we screened out 11 promising 2D BMSs from the 2DMatPedia database. Three of them are easily exfoliated from their bulk form, and two of them have proper ionic potential and electronic affinity which are suitable for bipolar doping. By analyzing their electronic structures, we ascribe the formation of BMS to the strong crystal field effect and low spin-exchange interaction. Moreover, we proposed that BMS can be obtained by stacking two half semiconductors with type-II band alignment and interlayer antiferromagnetic coupling. This approach was verified in CrI_3/VI_3 and CrSCl/CrSBr heterostructures. This spin-dependent transport phenomenon in BMSs will serve as a good platform in both fundamental research and applications of spintronic devices.

ASSOCIATED CONTENT

Supporting Information

The Supporting Information is available free of charge at https://pubs.acs.org/doi/10.1021/acsaelm.2c00464.

Energy difference between AFM and FM configurations for the screened BMS; phonon dispersions; band structures; charge density; band alignment; band structure for CrI_3/VI_3 and CrSCl/CrSBr heterostructures; lattice parameters; and details about generating magnetic structures, orbital ordering of VI_3, and interlayer coupling of CrSBr (PDF)

AUTHOR INFORMATION

Corresponding Author

Shixuan Du − *Beijing National Laboratory for Condensed Matter Physics, Institute of Physics, Chinese Academy of Sciences, Beijing 100190, China; School of Physics, University of Chinese Academy of Sciences, Beijing 100049, China; Songshan Lake Materials Laboratory, Dongguan, Guangdong 523808, China; CAS Center for Excellence in Topological Quantum Computation, University of Chinese Academy of Sciences, Beijing 100190, China;* orcid.org/0000-0001-9323-1307; Email: sxdu@iphy.ac.cn

Authors

Jun Deng − *Beijing National Laboratory for Condensed Matter Physics, Institute of Physics, Chinese Academy of Sciences, Beijing 100190, China;* orcid.org/0000-0003-2420-8079

Jinbo Pan − *Beijing National Laboratory for Condensed Matter Physics, Institute of Physics, Chinese Academy of Sciences, Beijing 100190, China; School of Physics, University of Chinese Academy of Sciences, Beijing 100049, China; Songshan Lake Materials Laboratory, Dongguan, Guangdong 523808, China*

Yanfang Zhang − *School of Physics, University of Chinese Academy of Sciences, Beijing 100049, China*

Yuhui Li − *Beijing National Laboratory for Condensed Matter Physics, Institute of Physics, Chinese Academy of Sciences, Beijing 100190, China; School of Physics, University of Chinese Academy of Sciences, Beijing 100049, China*

Wenhan Dong − *Beijing National Laboratory for Condensed Matter Physics, Institute of Physics, Chinese Academy of Sciences, Beijing 100190, China; School of Physics, University of Chinese Academy of Sciences, Beijing 100049, China*

Jiatao Sun − *School of Information and Electronics, MIIT Key Laboratory for Low-Dimensional Quantum Structure and Devices, Beijing Institute of Technology, Beijing 100081, China*

Complete contact information is available at: https://pubs.acs.org/10.1021/acsaelm.2c00464

Notes

The authors declare no competing financial interest.

ACKNOWLEDGMENTS

This work was supported by grants from the National Natural Science Foundation of China (Grant 61888102), the Major Program of National Natural Science Foundation of China (Grant 92163206), and the Strategic Priority Research Program of the Chinese Academy of Sciences (Grant XDB30000000). Y.Z. acknowledges the support of National

Natural Science Foundation of China (Grant 52102193) and the Fundamental Research Funds for the Central Universities. Computational resources were provided by the National Supercomputing Center in Tianjin.

REFERENCES

(1) Li, X.; Yang, J. First-principles design of spintronics materials. *Natl. Sci. Rev.* **2016**, *3* (3), 365−381.
(2) Degroot, R. A.; Mueller, F. M.; van engen, P. G.; Buschow, K. H. J. New Class of Materials: Half-Metallic Ferromagnets. *Phys. Rev. Lett.* **1983**, *50* (25), 2024−2027.
(3) Li, X.; Yang, J. Bipolar magnetic materials for electrical manipulation of spin-polarization orientation. *Phys. Chem. Chem. Phys.* **2013**, *15* (38), 15793−15801.
(4) Li, X.; Wu, X.; Li, Z.; Yang, J.; Hou, J. G. Bipolar magnetic semiconductors: a new class of spintronics materials. *Nanoscale* **2012**, *4* (18), 5680−5685.
(5) Li, X.; Wu, X.; Yang, J. Half-Metallicity in $MnPSe_3$ Exfoliated Nanosheet with Carrier Doping. *J. Am. Chem. Soc.* **2014**, *136* (31), 11065−11069.
(6) He, J.; Lyu, P.; Sun, L. Z.; Morales Garcia, A.; Nachtigall, P. High temperature spin-polarized semiconductivity with zero magnetization in two-dimensional Janus MXenes. *J. Mater. Chem. C* **2016**, *4* (27), 6500−6509.
(7) Sun, Y.; Zhuo, Z.; Wu, X. Bipolar magnetism in a two-dimensional NbS_2 semiconductor with high Curie temperature. *J. Mater. Chem. C* **2018**, *6* (42), 11401−11406.
(8) Zhang, J.; Zhao, B.; Ma, C.; Yang, Z. Bipolar ferromagnetic semiconductors and doping-tuned room-temperature half-metallicity in monolayer MoX_3 (X=Cl, Br, I): An HSE06 study. *Phys. Rev. B* **2021**, *103* (7), 075433.
(9) Li, X.; Yang, J. Toward Room-Temperature Magnetic Semiconductors in Two-Dimensional Ferrimagnetic Organometallic Lattices. *J. Phys. Chem. Lett.* **2019**, *10* (10), 2439−2444.
(10) Huang, B.; Clark, G.; Navarro-Moratalla, E.; Klein, D. R.; Cheng, R.; Seyler, K. L.; Zhong, D.; Schmidgall, E.; McGuire, M. A.; Cobden, D. H.; Yao, W.; Xiao, D.; Jarillo-Herrero, P.; Xu, X. Layer-dependent ferromagnetism in a van der Waals crystal down to the monolayer limit. *Nature* **2017**, *546* (7657), 270−273.
(11) Gong, C.; Li, L.; Li, Z.; Ji, H.; Stern, A.; Xia, Y.; Cao, T.; Bao, W.; Wang, C.; Wang, Y.; Qiu, Z. Q.; Cava, R. J.; Louie, S. G.; Xia, J.; Zhang, X. Discovery of intrinsic ferromagnetism in two-dimensional van der Waals crystals. *Nature* **2017**, *546* (7657), 265−269.
(12) Huang, C.; Feng, J.; Wu, F.; Ahmed, D.; Huang, B.; Xiang, H.; Deng, K.; Kan, E. Toward Intrinsic Room-Temperature Ferromagnetism in Two-Dimensional Semiconductors. *J. Am. Chem. Soc.* **2018**, *140* (36), 11519−11525.
(13) Gjerding, M. N.; Taghizadeh, A.; Rasmussen, A.; Ali, S.; Bertoldo, F.; Deilmann, T.; Knøsgaard, N. R.; Kruse, M.; Larsen, A. H.; Manti, S.; Pedersen, T. G.; Petralanda, U.; Skovhus, T.; Svendsen, M. K.; Mortensen, J. J.; Olsen, T.; Thygesen, K. S. Recent progress of the Computational 2D Materials Database (C2DB). *2D Mater.* **2021**, *8* (4), 044002.
(14) Zhou, J.; Shen, L.; Costa, M. D.; Persson, K. A.; Ong, S. P.; Huck, P.; Lu, Y.; Ma, X.; Chen, Y.; Tang, H.; Feng, Y. P. 2DMatPedia, an open computational database of two-dimensional materials from top-down and bottom-up approaches. *Sci. Data* **2019**, *6* (1), 86.
(15) Liu, H.; Meng, S.; Liu, F. Screening 2D materials with topological flat bands. *Phys. Rev. Mater.* **2021**, *5* (8), 084203.
(16) Yang, T.; Zhou, J.; Song, T. T.; Shen, L.; Feng, Y. P.; Yang, M. High-Throughput Identification of Exfoliable Two-Dimensional Materials with Active Basal Planes for Hydrogen Evolution. *ACS Energy Lett.* **2020**, *5* (7), 2313−2321.
(17) Wang, H.; Feng, Q.; Li, X.; Yang, J. High-Throughput Computational Screening for Bipolar Magnetic Semiconductors. *Research* **2022**, *2022*, 9857631.
(18) Pan, J.; Yu, J.; Zhang, Y.-F.; Du, S.; Janotti, A.; Liu, C.-X.; Yan, Q. Quantum anomalous Hall effect in two-dimensional magnetic insulator heterojunctions. *npj Comput. Mater.* **2020**, *6*, 152.
(19) Kresse, G.; Furthmuller, J. Efficiency of ab-initio total energy calculations for metals and semiconductors using a plane-wave basis set. *Comput. Mater. Sci.* **1996**, *6* (1), 15−50.
(20) Perdew, J. P.; Burke, K.; Ernzerhof, M. Generalized gradient approximation made simple. *Phys. Rev. Lett.* **1996**, *77* (18), 3865−3868.
(21) Kresse, G.; Joubert, D. From ultrasoft pseudopotentials to the projector augmented-wave method. *Phys. Rev. B* **1999**, *59* (3), 1758−1775.
(22) Dudarev, S. L.; Botton, G. A.; Savrasov, S. Y.; Humphreys, C. J.; Sutton, A. P. Electron-energy-loss spectra and the structural stability of nickel oxide: An LSDA+U study. *Phys. Rev. B* **1998**, *57* (3), 1505−1509.
(23) Ong, S. P.; Richards, W. D.; Jain, A.; Hautier, G.; Kocher, M.; Cholia, S.; Gunter, D.; Chevrier, V. L.; Persson, K. A.; Ceder, G. Python Materials Genomics (pymatgen): A robust, open-source python library for materials analysis. *Comput. Mater. Sci.* **2013**, *68*, 314−319.
(24) Monkhorst, H. J.; Pack, J. D. Special points for brillouin-zone integrations. *Phys. Rev. B* **1976**, *13* (12), 5188−5192.
(25) Heyd, J.; Scuseria, G. E.; Ernzerhof, M. Hybrid functionals based on a screened Coulomb potential. *J. Chem. Phys.* **2003**, *118* (18), 8207−8215.
(26) Togo, A.; Tanaka, I. First principles phonon calculations in materials science. *Scr. Mater.* **2015**, *108*, 1−5.
(27) Klimes, J.; Bowler, D. R.; Michaelides, A. Chemical accuracy for the van der Waals density functional. *J. Phys.: Condens. Matter* **2009**, *22* (22), 022201.
(28) Klimeš, J.; Bowler, D. R.; Michaelides, A. Van der Waals density functionals applied to solids. *Phys. Rev. B* **2011**, *83* (19), 195131.
(29) Jiang, P.; Wang, C.; Chen, D.; Zhong, Z.; Yuan, Z.; Lu, Z.-Y.; Ji, W. Stacking tunable interlayer magnetism in bilayer CrI_3. *Phys. Rev. B* **2019**, *99* (14), 144401.
(30) He, J.; Ma, S.; Lyu, P.; Nachtigall, P. Unusual Dirac half-metallicity with intrinsic ferromagnetism in vanadium trihalide monolayers. *J. Mater. Chem. C* **2016**, *4* (13), 2518−2526.
(31) Cococcioni, M.; de Gironcoli, S. Linear response approach to the calculation of the effective interaction parameters in the LDA+U method. *Phys. Rev. B* **2005**, *71* (3), 035105.
(32) Lu, M.; Yao, Q.; Xiao, C.; Huang, C.; Kan, E. Mechanical, Electronic, and Magnetic Properties of NiX_2 (X = Cl, Br, I) Layers. *Acs Omega* **2019**, *4* (3), 5714−5721.
(33) Zhao, P.; Ma, Y.; Lei, C.; Wang, H.; Huang, B.; Dai, Y. Single-layer $LaBr_2$: Two-dimensional valleytronic semiconductor with spontaneous spin and valley polarizations. *Appl. Phys. Lett.* **2019**, *115* (26), 261605.
(34) Bikaljevic, D.; Gonzalez-Orellana, C.; Pena-Diaz, M.; Steiner, D.; Dreiser, J.; Gargiani, P.; Foerster, M.; Nino, M. A.; Aballe, L.; Ruiz-Gomez, S.; Friedrich, N.; Hieulle, J.; Jingcheng, L.; Ilyn, M.; Rogero, C.; Pascual, J. I. Noncollinear Magnetic Order in Two-Dimensional $NiBr_2$ Films Grown on Au(111). *ACS Nano* **2021**, *15* (9), 14985−14995.
(35) Jiang, Z.; Wang, P.; Xing, J.; Jiang, X.; Zhao, J. Screening and Design of Novel 2D Ferromagnetic Materials with High Curie Temperature above Room Temperature. *ACS Appl. Mater. Interfaces* **2018**, *10* (45), 39032−39039.
(36) Peng, R.; Ma, Y. D.; Xu, X. L.; He, Z. L.; Huang, B. B.; Dai, Y. Intrinsic anomalous valley Hall effect in single-layer Nb_3I_8. *Phys. Rev. B* **2020**, *102* (3), 035412.
(37) Deng, J.; Guo, J.; Hosono, H.; Ying, T.; Chen, X. Two-dimensional bipolar ferromagnetic semiconductors from layered antiferromagnets. *Phys. Rev. Mater.* **2021**, *5* (3), 034005.
(38) Hosono, H. Exploring Electro-active Functionality of Transparent Oxide Materials. *Jpn. J. Appl. Phys.* **2013**, *52* (9), 090001.

https://doi.org/10.1021/acsaelm.2c00464
ACS Appl. Electron. Mater. 2022, 4, 3232−3239

(39) McGuire, M. A.; Dixit, H.; Cooper, V. R.; Sales, B. C. Coupling of Crystal Structure and Magnetism in the Layered, Ferromagnetic Insulator CrI_3. *Chem. Mater.* **2015**, *27* (2), 612−620.
(40) Kong, T.; Stolze, K.; Timmons, E. I.; Tao, J.; Ni, D.; Guo, S.; Yang, Z.; Prozorov, R.; Cava, R. J. VI_3-a New Layered Ferromagnetic Semiconductor. *Adv. Mater.* **2019**, *31* (17), No. 1808074.
(41) Tian, S.; Zhang, J.-F.; Li, C.; Ying, T.; Li, S.; Zhang, X.; Liu, K.; Lei, H. Ferromagnetic van der Waals Crystal VI_3. *J. Am. Chem. Soc.* **2019**, *141* (13), 5326−5333.
(42) Yang, K.; Fan, F.; Wang, H.; Khomskii, D. I.; Wu, H. VI_3: A two-dimensional Ising ferromagnet. *Phys. Rev. B* **2020**, *101* (10), 100402.
(43) Huang, C.; Wu, F.; Yu, S.; Jena, P.; Kan, E. Discovery of twin orbital-order phases in ferromagnetic semiconducting VI_3 monolayer. *Phys. Chem. Chem. Phys.* **2020**, *22* (2), 512−517.
(44) Nguyen, T. P. T.; Yamauchi, K.; Oguchi, T.; Amoroso, D.; Picozzi, S. Electric-field tuning of the magnetic properties of bilayer VI_3: A first-principles study. *Phys. Rev. B* **2021**, *104* (1), 014414.
(45) Wang, Y.-P.; Long, M.-Q. Electronic and magnetic properties of van der Waals ferromagnetic semiconductor VI_3. *Phys. Rev. B* **2020**, *101* (2), 024411.
(46) Jain, A.; Ong, S. P.; Hautier, G.; Chen, W.; Richards, W. D.; Dacek, S.; Cholia, S.; Gunter, D.; Skinner, D.; Ceder, G.; Persson, K. A. Commentary: The Materials Project: A materials genome approach to accelerating materials innovation. *APL Mater.* **2013**, *1* (1), 011002.
(47) Subhan, F.; Hong, J. Large Valley Splitting and Enhancement of Curie Temperature in a Two-Dimensional VI_3/CrI_3 Heterostructure. *J. Phys. Chem. C* **2020**, *124* (13), 7156−7162.
(48) Guo, Y.; Zhang, Y.; Yuan, S.; Wang, B.; Wang, J. Chromium sulfide halide monolayers: intrinsic ferromagnetic semiconductors with large spin polarization and high carrier mobility. *Nanoscale* **2018**, *10* (37), 18036−18042.
(49) Wang, C.; Zhou, X.; Zhou, L.; Tong, N.-H.; Lu, Z.-Y.; Ji, W. A family of high-temperature ferromagnetic monolayers with locked spin-dichroism-mobility anisotropy: MnNX and CrCX (X = Cl, Br, I; C = S, Se, Te). *Sci. Bull.* **2019**, *64* (5), 293−300.
(50) Guo, Y.; Zhang, Y.; Zhou, Z.; Zhang, X.; Wang, B.; Yuan, S.; Dong, S.; Wang, J. Spin-constrained optoelectronic functionality in two-dimensional ferromagnetic semiconductor heterojunctions. *Mater. Horiz.* **2021**, *8* (4), 1323−1333.
(51) Liu, N.; Zhou, S.; Zhao, J. Photoinduced Spin Injection and Ferromagnetism in 2D Group III Monochalcogenides. *J. Phys. Chem. Lett.* **2022**, *13* (2), 590−597.

https://doi.org/10.1021/acsaelm.2c00464
ACS Appl. Electron. Mater. 2022, 4, 3232−3239